

# SPECTROSCOPIC MEASUREMENTS OF SOLAR WIND GENERATION

John L. Kohl, George L. Withbroe, Carlos A. Zapata  
Harvard-Smithsonian Center for Astrophysics, Cambridge, MA 02138

and

Giancarlo Noci  
Istituto di Astronomia, Universita di Padova, Padova, Italy

## ABSTRACT

Spectroscopically observable quantities are described which are sensitive to the primary plasma parameters of the solar wind's source region. The method is discussed in which those observable quantities are used as constraints in the construction of empirical models of various coronal structures. Simulated observations are used to examine the fractional contributions to observed spectral intensities from coronal structures of interest which co-exist with other coronal structures along simulated lines-of-sight. The sensitivity of spectroscopic observables to the physical parameters within each of those structures is discussed.

## I. INTRODUCTION

High resolution spectroscopic measurements of UV, EUV and XUV radiation from the extended solar corona can provide highly constrained empirical models of the coronal plasma structures that produce solar wind. New spectroscopic diagnostic techniques are being developed to specify electron temperatures and densities, ion velocity distributions and densities, outflow velocities of coronal particles into the solar wind, chemical abundances and vector magnetic fields.

Although spectroscopic measurements are somewhat less straightforward to interpret than *in situ* measurements, their use in astrophysics and in controlled thermonuclear research is well established as a powerful means of determining the properties of plasmas that may not be amenable to *in situ* techniques. The usual approach for interpreting spectroscopic data is to develop a model of the plasma of interest that is constrained by the values of observable quantities. Ideally, each observable is sensitive to and governed by a specific plasma parameter (e.g. a spectral line profile that is primarily controlled by the velocity distribution of the corresponding particle species). Empirical models that are used to specify plasma parameters and their spatial variations are relatively unconstrained by theory, take into account the basic physics of spectral line formation, and treat the line-of-sight contributions in a self consistent manner. Such models do not depend upon, nor specify, the physical processes that may be operating within the plasma such as the energy and momentum transport and deposition mechanisms. The model is an empirical description of the observed plasma and specifies throughout the plasma structure, the local values of the basic plasma parameters (e.g. particle velocities and densities). To establish a high level of confidence in a model it is necessary to determine a large number of partially redundant observational constraints

which are sensitive to all of the primary plasma parameters and to require the model to reproduce all of the measured spectroscopic quantities.

Once the derived plasma parameters are specified in this way, they can be introduced into more sophisticated models which contain a theoretical description of probable physical processes that may be responsible for maintaining the properties of the plasma of interest. These models inevitably lead to an improved understanding of the physics of the observed plasma because the empirical constraints result in the rejection of candidate physical processes whose presence would be inconsistent with the observations. With an increasing number of empirical constraints, the range of possible physical models is narrowed and a meaningful understanding of the nature of the plasma of interest can be established.

In the case of the solar wind acceleration regions of the solar corona, empirically derived knowledge of plasma conditions has been extremely limited, and, hence, energy and momentum deposition processes as well as the principal mechanisms for energy and momentum transport (other than radiation and thermal conduction) have not been identified. Spectroscopic measurements of open and closed magnetic structures of the extended corona and detailed modeling can help to establish the identity and magnitude of transport and deposition processes operating in representative coronal structures, thus improving the understanding of the physics of solar wind acceleration and determining the role of different types of coronal structures in the production of the solar wind. Observations of a broad range of ionic species in different structures may help to explain abundance enhancements that have been observed in solar wind streams at 1 AU (Hirshberg, 1975). Improved knowledge of the physical conditions in the solar wind acceleration region may also lead to a better understanding of interactions between magnetic fields and low density flowing plasmas, both for steady-state flow and coronal transients.

The spectroscopic techniques that we are developing to study the physics of the source regions of the solar wind have been described elsewhere (Kohl and Withbroe, 1982; Withbroe *et al.*, 1982a) and will be only briefly identified here. The primary purpose of this paper is to discuss the approach that is being used to interpret the observations; in particular, the analysis of the line-of-sight contributions to the emergent coronal intensities and the sensitivity of specific observables to the plasma parameters of representative coronal structures. The final section includes a brief summary of our initial ultraviolet spectroscopic measurements of the extended corona from sounding rockets and our plans for more extensive measurements.

## II. SPECTROSCOPIC DIAGNOSTICS

The spectroscopic diagnostics that we are developing for the solar wind acceleration region of the extended corona (radii  $> 1.3 R_{\odot}$  from sun center) make use of information contained in measurements of the intensities and profiles of spectral features in the UV, EUV and XUV wavelength ranges. Because the particle densities in the extended corona are low, the thermalization and ionization equilibrium times are long and, hence, the various particle species such as electrons, protons and other ions have velocity distributions that are not characterized by the same temperature and have ionization distributions that are frozen-in at various heights. Several physical processes that have

been suggested as possibilities for energy and momentum transport (e.g. Alfvén and MHD fast mode waves) affect in characteristic ways the particle velocity distributions as a function of height. A knowledge of the velocity distributions of particles of unlike mass would help to distinguish thermal velocity components from nonthermal velocities due to energy and momentum transport processes (e.g. the transverse velocities of propagating waves). If the large number of plasma parameters required to describe the solar wind acceleration region are to be studied spectroscopically, it is necessary to measure a diversity of spectral features that are sensitive to the velocity distributions and densities of each of the major and some minor constituents of the solar wind plasma, and also to measure spectral quantities that are sensitive to a broad range of outflow velocities. In order to understand the role of the coronal magnetic fields, it would be extremely advantageous to determine coronal values of that quantity.

A meaningful representation of a coronal plasma must include, among others, descriptions of the behavior of the two major constituents, the protons and the electrons. The electron density has traditionally been determined from observations of electron scattered visible light and this continues to be the best method. A measurement of electron density together with the plasma neutrality condition and an estimate of the chemical abundance and ionization balance of helium permit a straightforward determination of proton density in a model.

#### Random Velocity Diagnostics from H I Lyman- $\alpha$

Measurements of the line profiles of resonantly scattered and electron scattered H I Lyman- $\alpha$  radiation in the corona are very sensitive to the velocity distributions of the protons and the electrons, respectively. The resonantly scattered component depends upon the scattering of chromospheric Lyman- $\alpha$  photons by neutral hydrogen atoms in the corona. Even though the ratio of neutral hydrogen to free protons is about  $10^{-7}$  at coronal temperatures and densities (Gabriel, 1971), the large coronal proton abundance coupled with the high intensity of the chromospheric Lyman- $\alpha$  radiation gives rise to a coronal resonantly scattered component of Lyman- $\alpha$  that is strong enough to be measured out to large distances above the solar surface. The formation of the resonantly scattered Lyman- $\alpha$  line has been described by Gabriel (1971), Beckers and Chipman (1974) and Withbroe *et al.* (1982a). Because the tenuous coronal plasma is optically thin to ultraviolet radiation, an observed Lyman- $\alpha$  profile is a direct measurement of the run of H I velocities along the line-of-sight. This velocity distribution includes the thermal motions, nonthermal motions such as the transverse velocities of propagating waves and the components of the outflow velocities along the line-of-sight. Since the thermal velocities of hydrogen at coronal temperatures are relatively large ( $160 \text{ km s}^{-1}$  for a thermal temperature of  $1.5 \times 10^6 \text{ K}$ ), thermal motions are expected to be a major contributor to coronal H I velocity distributions.

The profile of the resonantly scattered component of H I Lyman- $\alpha$  is also a measure of the velocity distribution of protons in regions where the coronal expansion time is much longer than the characteristic time for charge exchange between hydrogen atoms and protons. For  $r < 8 R_{\odot}$  in quiet coronal regions and  $r < 3 R_{\odot}$  in low density coronal holes, the proton and hydrogen velocities are expected to be nearly identical and, hence, the profile of the resonantly

scattered H I Lyman- $\alpha$  line can be used in models to constrain both the H I and proton velocity distributions (Withbroe *et al.*, 1982a).

The electron scattered component of the coronal H I Lyman- $\alpha$  line is much weaker (by about 3 orders of magnitude) than the resonantly scattered component and has a FWHM  $\approx 50$  Å compared to the  $\approx 1$  Å width of the resonantly scattered profile. It is produced in the corona by Thomson scattering of chromospheric H I Lyman- $\alpha$  radiation. The formation of electron scattered Lyman- $\alpha$  has been discussed by Withbroe *et al.* (1982a). Calculated profiles provided in Figure 4 of that reference show that the shape of the profiles are very sensitive to the velocity distribution of coronal electrons. The line profile of the electron scattered radiation is a stronger function of the scattering geometry than is the resonantly scattered profile.

### Random Velocities and Densities from Other Lines

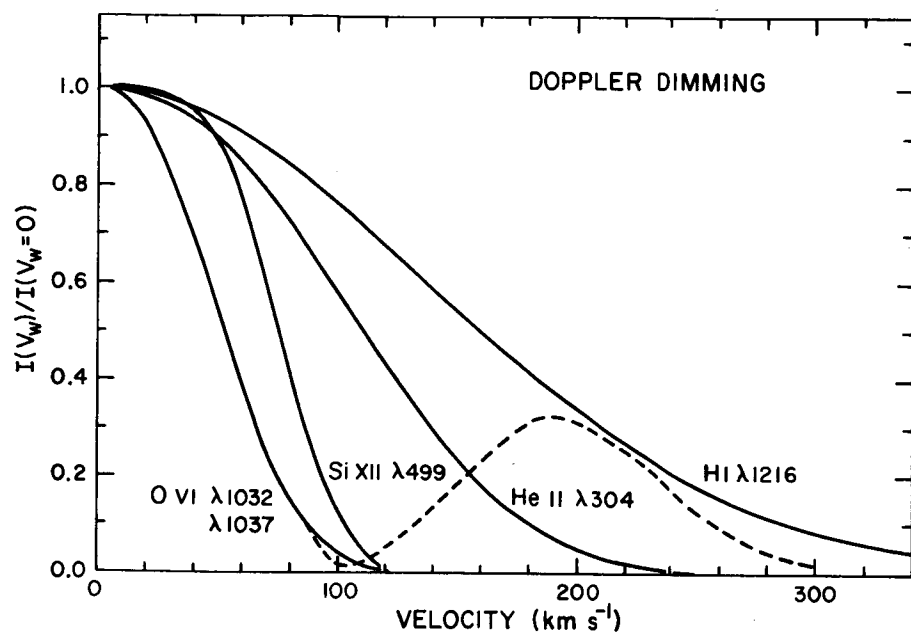
Profiles of the spectral lines of ions such as C IV, N V, O VI, Ne VIII, Mg X, Si XII, Fe XII and He II which should be observable in the corona out to  $r = 3$  to  $5 R_{\odot}$ , can yield information on the velocity distributions of those particles (Kohl and Withbroe, 1982). For most of the UV, EUV and XUV lines, the emergent intensity is a combination of collisionally excited and resonantly scattered components. For ions that are more massive than H I, the thermal component of the velocity distribution in the corona is not expected to be as large as for hydrogen. Hence, the profiles of those systems are expected to be sensitive to nonthermal velocities and, in the case of the more massive species, to be dominated by them. The ability to distinguish between thermal and nonthermal velocities is probably the key to discovering the identities of energy and momentum transport processes that are expected to impart characteristic velocities to the coronal ions.

It is highly desirable to determine the relative intensities of the collisionally excited and resonantly scattered components of a spectral line because the former component is sensitive to the density of the corresponding ion and the latter to outflow velocity. In the case of Li-like resonance lines (Kohl and Withbroe, 1982), the respective contributions from each mechanism can be determined from the ratio of the intensities of the  $2s \ ^1S_{1/2} - 2p \ ^2P_{3/2}$  and  $2s \ ^1S_{1/2} - 2p \ ^2P_{1/2}$  fine structure lines (e.g. O VI  $\lambda 1032$  and  $\lambda 1037$ ). For the case where the resonantly scattered components of the lines are being pumped by radiation from identical ions in deeper layers of the solar atmosphere, the resonantly scattered components will have a 4:1 ratio while the collisionally excited components of the lines will have a 2:1 ratio.

### Outflow Velocity Diagnostics

The intensity of the resonantly scattered component depends upon the number of particles along the line-of-sight that are capable of scattering radiation in the spectral line and upon the intensity of the incoming radiation. The intensity of scattered photons is a function of the net outflow velocity of coronal scatterers. This can be understood by considering a static atmosphere where the central wavelength of the coronal scattering profile is identical to that of the incoming radiation and the case of an outflowing plasma where the incoming radiation is red-shifted off the center of the scattering profile. In

the former case there will be a maximum amount of resonant scattering and in the latter, the amount of resonant scattering will decrease with increasing velocity. Notice that spectral lines of unlike widths are sensitive to different ranges of outflow velocity. This intensity dependence, termed Doppler-dimming (Hyder and Lites, 1970; Beckers and Chipman, 1974), provides the sensitivity of observable quantities that is needed to constrain the values of outflow velocities in a model of an observed coronal structure. In Figure 1, we see that the H I Lyman- $\alpha$  line is sensitive to flow velocities greater than 100 km s<sup>-1</sup> while the O VI  $\lambda$ 1032 line is sensitive to velocities in the 30-100 km s<sup>-1</sup> range and the other lines are sensitive to somewhat larger velocities.



The Doppler-dimming of the O VI line at 1037.587 Å is particularly interesting because the resonantly scattered component of this line can be pumped either by O VI  $\lambda$ 1037 radiation from deeper atmospheric layers or by the C II line at 1037.018 Å (Noci, Kohl and Withbroe, 1983). Pumping by the latter line occurs when the outflow velocity is large enough that the incoming C II profile is red shifted in the coronal ion rest frame by an amount that is large enough to make the incoming C II radiation profile and the O VI  $\lambda$ 1037 scattering profile overlap. The

Figure 1. Doppler dimming calculated as a function of flow velocity for the resonantly scattered components of several spectral lines. The solid O VI curve applies to both the  $\lambda$ 1031.766 and  $\lambda$ 1037.587 lines. For velocities greater than 120 km s<sup>-1</sup>, the resonantly scattered intensity of  $\lambda$ 1031.766 Å approaches zero, but the  $\lambda$ 1037.587 Å intensity begins to increase due to pumping by the chromospheric C II line at 1037.018 Å as indicated by the dashed curve.

dashed line in Figure 1 shows the effect of the C II line on the velocity dependence of the O VI  $\lambda$ 1037 line. Because of this effect, the ratio of the intensities of the coronal O VI  $\lambda$ 1032 and  $\lambda$ 1037 lines as a function of radial height in the corona provides a very useful diagnostic of coronal outflow velocities that is illustrated in Figure 2. At low heights where velocities are small, the coronal O VI lines are formed by both resonant scattering from incoming O VI radiation and collisional excitation and the ratio is between 2 and 4. As the velocity increases with height, the resonant scattering of incoming O VI radiation is Doppler-dimmed in both the  $\lambda$ 1032 and  $\lambda$ 1037 lines and C II pumping of the  $\lambda$ 1037 line begins to decrease the  $\lambda$ 1032/ $\lambda$ 1037 ratio. At  $\rho = 1.5$  the  $\lambda$ 1037 resonantly scattered intensity from O VI and C II pumping are about equal. At even greater heights, the resonant scattering component of the  $\lambda$ 1037 line due to C II begins to dominate and the ratio becomes very small. At larger heights where the velo-

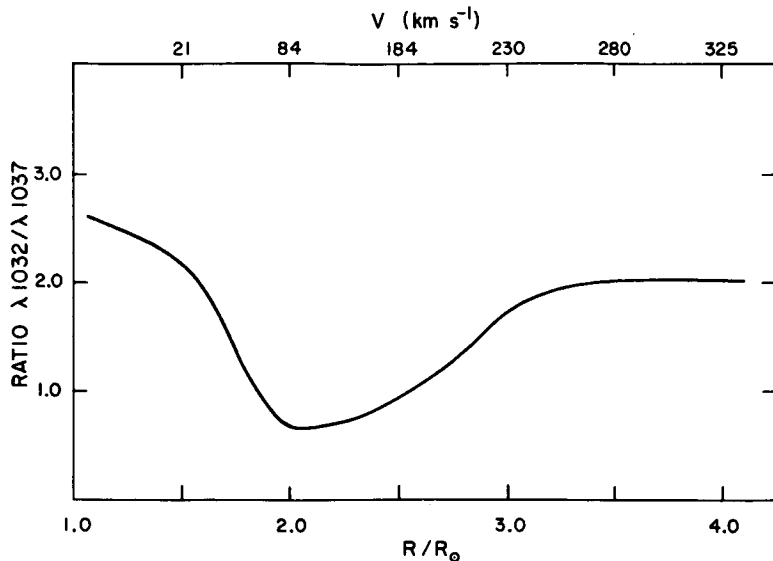


Figure 2. Calculated ratio of the intensities of the O VI  $\lambda 1032$  and  $\lambda 1037$  lines as a function of height for the indicated coronal hole velocities of Munro and Jackson (1977).

( $r \lesssim 1.5 R_{\odot}$  where the magnetic pressure generally exceeds the gas pressure) appears to control the location, size and shape of coronal holes and streamers. At greater heights the coronal magnetic field is swept into interplanetary space. The spatial variations of coronal densities, and most likely other plasma parameters such as temperatures, also appear to be strongly influenced by coronal magnetic fields which can channel energy carried by waves and/or electron thermal conduction. In addition, solar flares and coronal transients probably have magnetic origins. A possibility to use the Hanle effect (Hanle, 1924; Mitchell and Zemansky, 1934) for magnetic field diagnostics in astrophysics was originally suggested by Hyder (1965). Quantitative approaches have been described more recently. In particular, Bommier and Sahal-Br  chet (1982) have computed the effect of a magnetic field on the linear polarization of resonantly scattered H I Lyman- $\alpha$ . Coronal Lyman- $\alpha$ , which has been observed out to  $3.5 R_{\odot}$  using coronagraphic techniques (Kohl *et al.*, 1980), is polarized in the absence of a magnetic field. The Hanle effect is the modification of this linear polarization, due to the presence of the magnetic field. Bommier and Sahal-Br  chet provide analytical formulae which describe the Hanle effect for H I Lyman- $\alpha$ . In principle, those formulae could be used in models to specify the degree of polarization and the polarization direction of H I Lyman- $\alpha$  for a given coronal magnetic field configuration. Although the H I Lyman- $\alpha$  line is only sensitive to fields greater than about 6 gauss, other members of the H I Lyman series are sensitive to smaller fields.

### III. SENSITIVITY OF OBSERVABLES AND LINE-OF-SIGHT EFFECTS

For the purpose of discussing the line-of-sight contributions to the spectroscopic observables and for demonstrating the sensitivity of those observables to the basic physical quantities which describe a coronal structure, we use a model which specifies the temperatures, densities and outflow velocities of the electrons and protons as a function of height in several coronal structures that can be located at selected positions along the line-of-sight of a simulated observation (see Figure 3). With this model the contributions to the spectral

city is large enough to shift the C II line beyond the O VI  $\lambda 1037$  line, only the collisional components remain and the ratio again becomes 2.

### Magnetic Field Diagnostics

Of all the physical quantities that describe the extended coronal plasma, the magnetic field may be the most significant, but also it is one of the most difficult to measure. The magnetic field appears to influence strongly the structure of the corona and its outward extension into the heliosphere. The strength and configuration of the magnetic field in the low corona

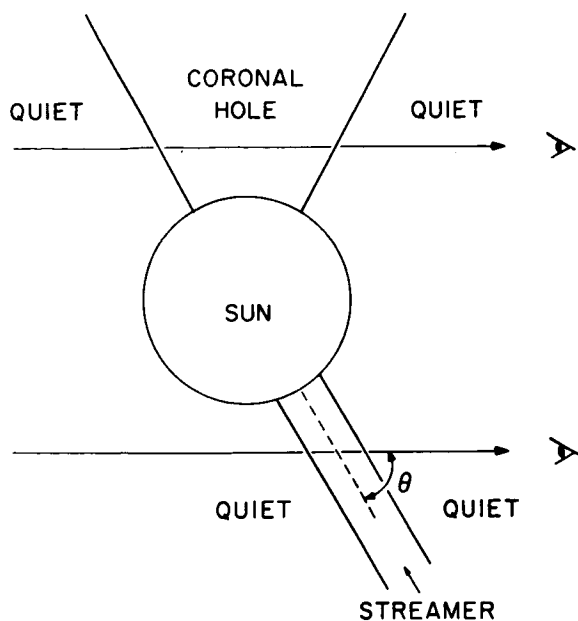


Figure 3. The geometry of simulated observations of a coronal hole surrounded by quiet coronal regions and of a coronal streamer.

given by Munro and Jackson (1977) with an absolute scale that is a specified multiple of their values. The electron temperature is taken to have a  $r^{-2/7}$  dependence and the absolute scale is normally taken from Withbroe *et al.* (1982a, Figure 11). Their values of electron temperature (e.g.  $1.5 \times 10^6$  K at  $r = 1.76 R_{\odot}$ ) were estimated from ratios of the H I Lyman- $\alpha$  and white light intensities. The ratios depend upon the ionization balance of hydrogen which is primarily a function of electron temperature. The proton and hydrogen random velocity distributions are assumed to be Maxwellian and to be characterized by the H I temperatures given by Withbroe *et al.* (1982a, Figure 11) who based their values upon measurements of H I Lyman- $\alpha$  profiles. In some cases, we specify an incremental change in the temperature.

For models of quiet coronal regions, the electron densities are Allen's values for an equatorial region at solar minimum; the outflow velocities are calculated assuming conservation of mass flux in spherical symmetry with  $100 \text{ km s}^{-1}$  at  $4.5 R_{\odot}$ ; the electron temperature is normally taken from Withbroe *et al.* (1982b, Figure 7) and the proton and hydrogen random velocity distributions are from the same source. The streamer model is similar to that of the quiet corona except the electron densities are taken to be 5 times Allen's (1963) equatorial values for solar minimum.

### Basic Geometry of Simulations

The geometry of the simulated observations is shown in Figure 3 where the plane of the figure lies at a position angle of  $90^\circ$  (i.e. the apparent equatorial plane). The height of observation  $\rho$  is the radial height in solar radii where the line-of-sight intersects the "plane of the disk" (i.e. the plane which is

line intensity profile of H I Lyman- $\alpha$  are calculated for volume elements along the line-of-sight. All outflow velocities are taken to be directed radially outward. Neutral hydrogen atoms are assumed to behave identically to the protons and the ionization balance of hydrogen is taken from Gabriel (1971). Only observations of H I Lyman- $\alpha$  are considered here, although the line-of-sight effects for observations of ions would be similar.

For models of coronal holes, we use Allen's (1963) electron density gradient for a polar region at solar minimum. For each of the two coronal holes that are discussed, we adopt an absolute scale which is chosen to be an integral multiple of Allen's absolute scale. The resulting densities are roughly based on the empirical values of Munro (1983) for coronal holes of a similar size. The outflow velocities are taken to have the radial dependence

perpendicular to the line-of-sight and passes through sun center). Angles  $\theta$  are measured from the line-of-sight to radial lines passing through specified locations in coronal structures. Observations of several coronal structures were simulated for the present study but most of the following discussion refers to the line-of-sight and coronal structures shown in the upper half of Figure 3. The structure of interest there is the coronal hole with radial boundaries between it and two quiet coronal regions. The  $\theta$  angle of the axis of symmetry is  $90^\circ$  and the boundaries are at  $\pm 30^\circ$  from the center line. This is a typical polar coronal hole for the declining phase of the cycle and is similar to one we observed during our July 20, 1982 rocket flight (Kohl et al., 1982). Broader holes are commonly found nearer to solar minimum (e.g. the 1973 polar coronal hole that was described by Munro and Jackson (1977) had boundaries at  $\pm 70^\circ$  from its center line). Smaller coronal hole-like structures also exist, especially in polar regions near the time of solar maximum. We observed a region on February 16, 1980 that had boundaries of about  $\pm 15^\circ$  from its center line. A similar structure is considered in Figure 4 and in the related discussion. The geometry of a simulated streamer observation is shown in the lower half of Figure 3. The streamer has cylindrical geometry with the axis of symmetry at angle  $\theta$ . Radial lines passing through the boundaries of the streamer at  $r = 1.5 R_\odot$  would subtend an angle of  $18^\circ$ . The streamer is surrounded by quiet corona.

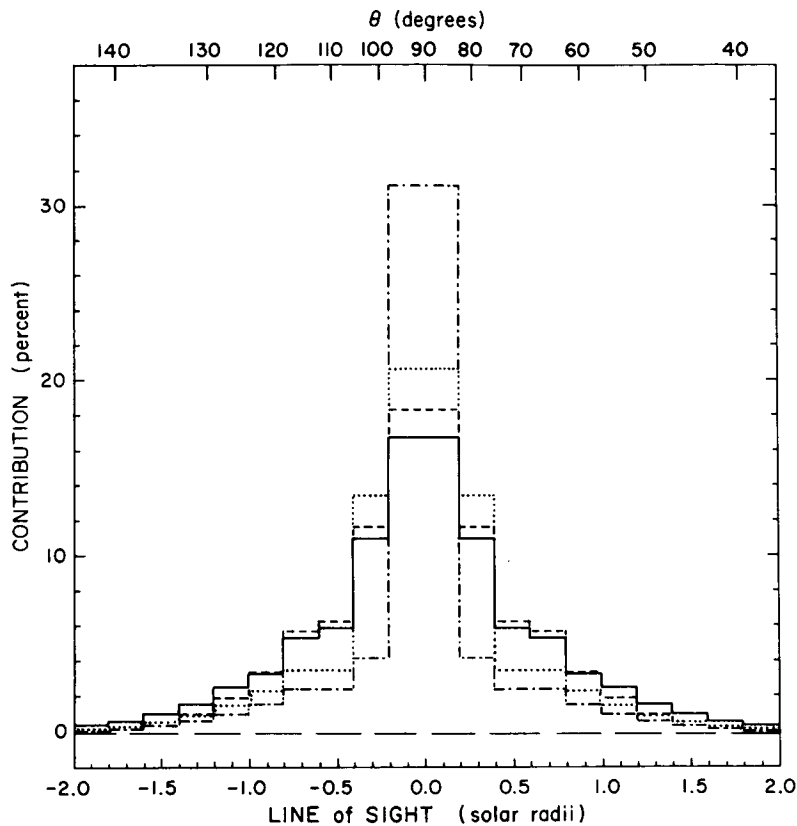


Figure 4. Contributions to observed intensities of H I Lyman- $\alpha$  for volume elements of  $0.2 R_\odot$  lengths which are located along the line-of-sight. Curves are plotted for simulated observations of a spherically symmetric corona (dash), a  $60^\circ$  coronal hole (solid line), a  $30^\circ$  coronal hole (dots) and a streamer at  $\theta = 90^\circ$  (dot-dash).

#### Fractional Contributions of Structures Along Line-of-Sight

If a spectroscopic observable is suitable for constraining the local values of a physical quantity in a model, then the contribution to that observable from the coronal structure of interest should be significant compared to the contributions from other regions. This is particularly important for the observations of line profiles, but as we shall see in Figure 6, is not quite as important for the line intensity. Figure 4 provides the fractional contribution to the intensity of H I Lyman- $\alpha$  from volume elements which have lengths of  $0.2 R_\odot$  along the line-of-sight. The lines-of-sight for the observations of Figure 4 intersect the plane of the disk at  $\rho = 1.5$ . The contributions are plotted against the

distance of the volume element from the plane of the disk in solar radii. The angles  $\theta$  to the centers of the individual volume elements are also provided.

The solid line histogram in Figure 4 refers to the corona illustrated in the upper part of Figure 3. The  $60^\circ$  wide coronal hole has a center line at  $\theta = 90^\circ$ . Its plasma parameters are the values for a coronal hole that were discussed earlier. The radial variations of the outflow velocity are taken to be identical (i.e. multiplier of one) to those of Munro and Jackson (1977) and the multiplier for density is 2 (i.e. densities twice as high as those in Allen's model for polar minimum). The hole is surrounded by a quiet coronal region with the parameters described earlier. The maximum contribution from a volume element is about 17% in this case and the fractional contribution from the coronal hole is 82% with the remaining 18% being contributed by the surrounding quiet corona. For a spherically symmetric corona with the same plasma parameters as the coronal hole, the fractional contribution would be 87% from the same region of space occupied by the coronal hole (i.e.  $60^\circ \leq \theta \leq 120^\circ$ ). The fractional contribution from a smaller coronal hole with boundaries at  $\theta = 75^\circ$  and  $105^\circ$ , and the same outflow velocities but with a density multiplier of 4 (twice the value for the previous example) is 69%. In each of these instances the structures of interest provide the dominant contribution and so for similar coronal holes or larger ones, the Lyman- $\alpha$  intensity and line profile at  $\rho = 1.5$  should be controlled by the parameters of the coronal hole and not by any surrounding quiet regions. Figure 4 also provides the contributions for a small streamer that is identical to the one shown in Figure 3 except that the center line is at  $\theta = 90^\circ$ . The total contribution from the streamer is 64% with the surrounding quiet corona providing the remaining 36%. Although it is not shown in Figure 4, we also calculated, for  $\rho = 1.5$ , the total streamer contributions for the cases where the streamer was centered at  $\theta = 60^\circ$  and  $30^\circ$ . The fractional contributions to the streamer in those cases are 40% and 18%, respectively. Those reduced contributions are due to the smaller densities at the observed radial heights in the streamer. This example illustrates the desirability of observing structures of interest that are located near the plane of the disk.

#### Sensitivity to Outflow Velocity

Recall from the discussion of spectroscopic diagnostics, that the resonantly scattered intensity is affected by the outflow velocity. For an observation of the corona depicted in the upper half of Figure 3, the fractional contribution from the coronal hole is plotted in Figure 5 for several absolute scales of outflow velocity. The coronal hole density multiplier is 2. The outflow velocities versus height for a multiplier of one times the Munro and Jackson (1977) values are indicated in the figure. In the case of zero outflow in the coronal hole, the fractional contribution from the hole decreases with increasing  $\rho$  because the adopted density gradient is larger in the hole than in the surrounding quiet corona. Because Doppler-dimming reduces the intensity of H I Lyman- $\alpha$ , the total contribution from the coronal hole decreases with increasing outflow velocity. Due to the small velocities encountered by observations at  $\rho = 1.5$ , the hole contribution at that height is  $>80\%$  for every curve of Figure 5. For the Munro-Jackson velocity scale, the contribution reaches 36% at  $\rho = 2.5$  and 25% (not shown) at  $\rho = 3.0$ . Of course, broader holes, such as the 1973 polar hole modelled by Munro and Jackson (1977), would tend to contribute larger fractional amounts to the observed intensity.

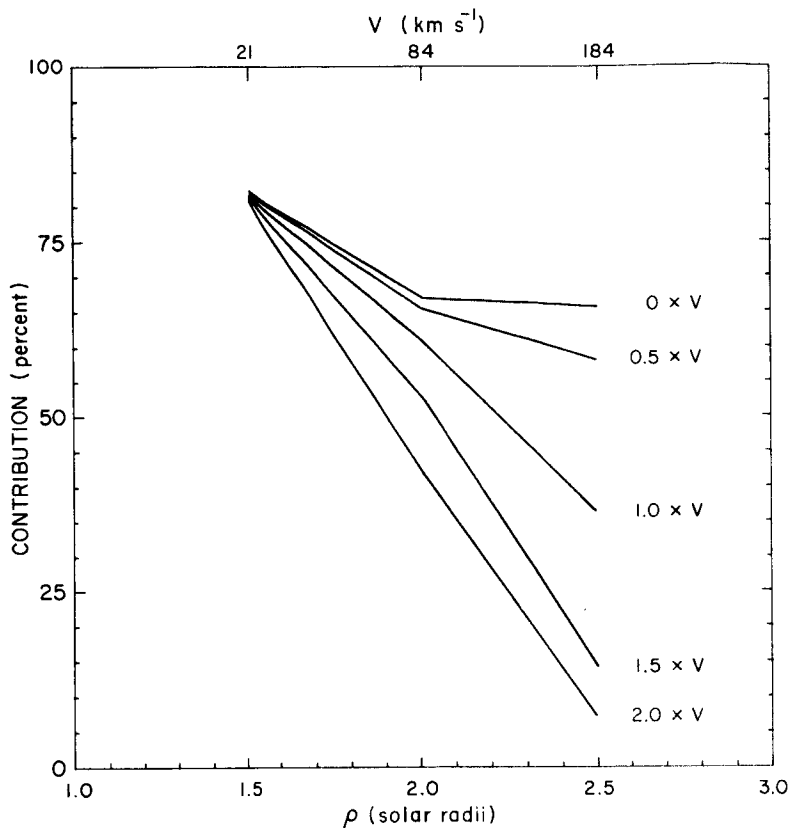


Figure 5. Total fractional contributions from the coronal hole for observations of a simulated  $60^\circ$  coronal hole surrounded by quiet coronal regions. Curves are plotted for outflow velocities in the hole that are 0.0, 0.5, 1.0, 1.5 and 2.0 times the outflow velocities of Munro and Jackson (1977).

Figure 6 is a plot of the observed Lyman- $\alpha$  line intensity versus  $\rho$  for the same  $60^\circ$ -wide coronal hole and surrounding region that were discussed in reference to Figure 5. Figure 6 illustrates the sensitivity of the observed H I Lyman- $\alpha$  intensity to the outflow velocity in the hole for the case where it is surrounded by a more dense coronal structure. For  $\rho = 2.5$  the observed intensity for zero outflow is about 1.8 times the value for the Munro and Jackson velocity scale and about 2.4 times the intensity for 1.5 times those velocities. Notice that the observed intensity is sensitive to outflow even in the case where the fractional contribution from the coronal hole is fairly small (see Figure 5). Also note that the observed intensity for  $\rho = 1.5$  is fairly insensitive to the range of outflow velocities that are expected at the contributing heights of that observation. This can also be seen from Figure 1. Therefore, the observed intensity at a given height relative to the intensity at  $\rho = 1.5$  is an observable quantity which is particularly sensitive to outflow velocity.

The situation is similar for observations of other lines although in the case of the O VI  $\lambda 1032$  and  $\lambda 1037$  lines, the sensitivity to small velocities makes an observation at  $1.3 R_\odot$  highly desirable for ensuring an observable intensity that is insensitive to expected outflow velocities. In the case of those lines, there is the added advantage of observing their line ratio as described earlier.

#### Sensitivity to Hydrogen Random Velocities

The primary purpose of Figure 7 is to demonstrate the sensitivity of observed Lyman- $\alpha$  profiles to the hydrogen random velocity distribution in a coronal structure of interest that co-exists with other structures along the line-of-sight. For this purpose we again consider the  $60^\circ$  coronal hole and surrounding quiet corona shown in Figure 3. Representative portions of line profiles are plotted in Figure 7 for simulated observations at  $\rho = 2.0$ . The profiles have a

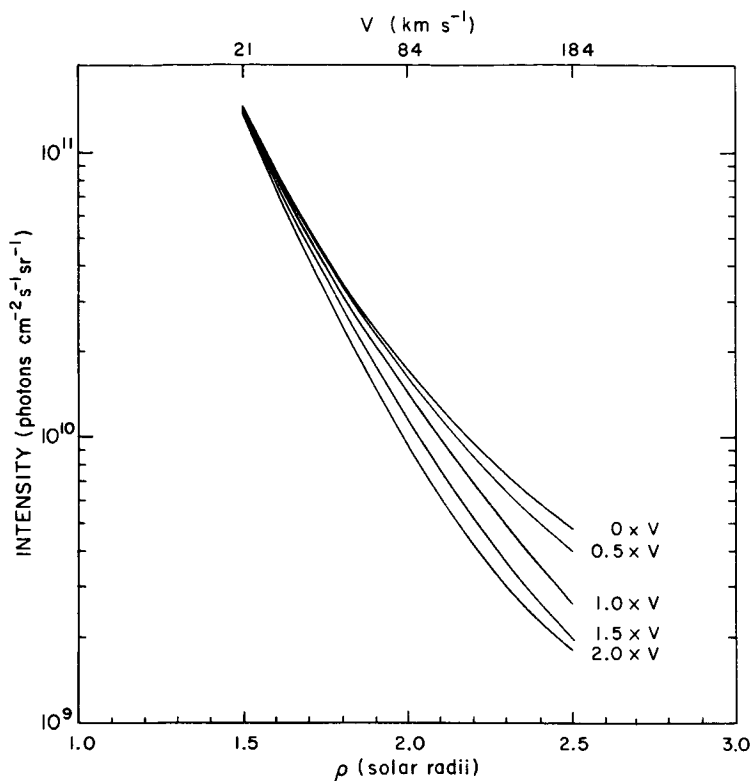


Figure 6. H I Lyman- $\alpha$  line intensities for simulated observations of a  $60^\circ$  coronal hole surrounded by quiet coronal regions. Curves are plotted for the outflow velocities of Figure 5.

relative intensity scale normalized to the intensities at line center. The primary observations to be considered here are line profiles for several different absolute scales of outflow velocity in the coronal hole (multipliers of 0, 1 and 2 times the Munro and Jackson scale). Those simulated profiles are compared in Figure 7 to other observations where the value of certain parameters in the coronal hole or in the quiet corona are changed from their normally adopted values. For the primary observations (represented by the solid curves), the increase in line width with increasing outflow velocity is due to the components of that velocity along the line-of-sight. Even for a velocity multiplier of two (corresponding to  $168 \text{ km s}^{-1}$  at  $2 R_\odot$ ) the fractional increase in width at  $e^{-1} I_0$ , due to this effect, is only 2%. Although this effect should be included in the models, the profiles are relatively insensitive to outflow velocities.

For the purpose of discussing the sensitivity of the observed profiles to the random velocity of hydrogen atoms and protons, it is convenient to parameterize the random coronal velocity by defining an effective hydrogen temperature which specifies a Doppler width for the adopted hydrogen velocity distribution. For coronal holes, the value of this parameter is taken to be  $1.4 \times 10^6 \text{ K}$  at  $2.0 R_\odot$  (Withbroe *et al.*, 1982a). A value of  $2.1 \times 10^6 \text{ K}$  (Withbroe *et al.*, 1982b) is adopted for that height in the quiet coronal region. The only difference in the model between the group of solid profile segments in Figure 7 and the group of dashed curves is that, for the latter curves, the effective temperature in the hole was increased by  $2 \times 10^5 \text{ K}$  at all heights. By comparing the dashed curve for zero outflow velocity to the corresponding solid curve, it is immediately obvious that the observed profiles are very sensitive to small differences in the random velocity distribution of hydrogen within the coronal hole. Similar comparisons for the profiles corresponding to the two non-zero outflow velocities indicate that the observed profiles are only slightly less sensitive in those cases. The reason for the slight decrease in sensitivity with increasing velocity is primarily because Doppler-dimming decreases the contribution from the coronal hole (see Figure 5). The smaller separations among the dashed curves compared to those among the solid curves is due to the domination of the random velocities over the outflow velocities in the hotter coronal hole models. The dotted profile in Figure 7 is for the case where the effective hydrogen temperature is increased in the quiet region by  $2 \times 10^5 \text{ K}$  while the

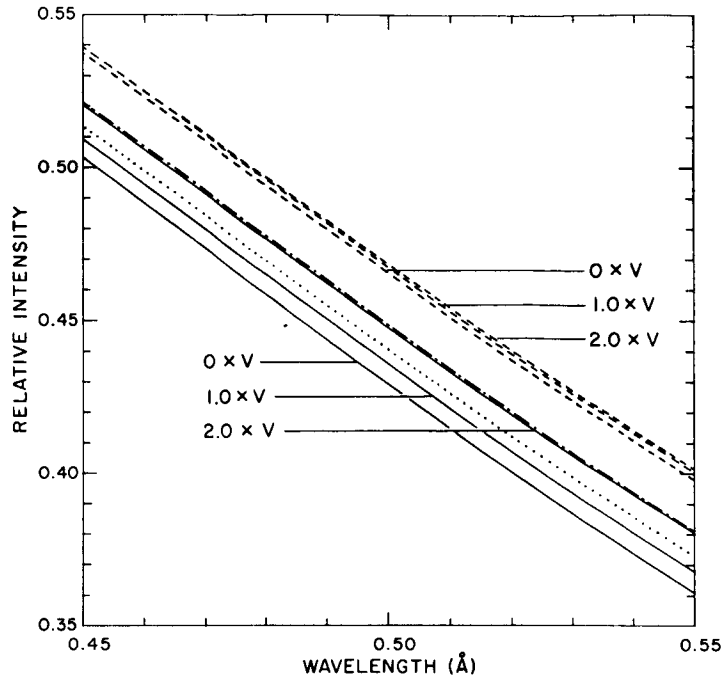


Figure 7. Segments of H I Lyman- $\alpha$  profiles for simulated observations of structures described in the text.

coronal hole has a velocity scale multiplier of one and has the other normally adopted parameters. This profile is only slightly wider than the corresponding profile (middle solid curve) for the usual effective temperature in the quiet region. This illustrates that the observed profiles are not overly sensitive to the effective temperature of the surrounding quiet corona.

A pure Gaussian profile (dot-dash curve) corresponding to the adopted random velocity distribution in the coronal hole at  $r = 2.0 R_{\odot}$  is also plotted. It is clear from a comparison to this profile that the line-of-sight effects, including the physics of the resonant scattering process, do not produce extremely large departures in the profile shapes from the simple profile that would be emitted by a hydrogen gas with the velocity distribution of the coronal hole at the height of observation.

#### IV. SUMMARY

Spectroscopic observables, including the line profiles and intensities of resonantly scattered and collisionally excited radiation from atoms and ions and the electron scattered profile of H I Lyman- $\alpha$ , are sensitive to all of the primary plasma parameters of the outflowing solar wind plasma in the extended solar corona. Individual observables have been identified that tend to be controlled, primarily, by particular plasma parameters. Therefore, in many respects, a measurement of a particular spectroscopic quantity can be considered to be a direct determination of the corresponding plasma parameter. However, the more rigorous approach, that has been emphasized in this paper, is to treat the observable quantities as constraints on an empirical model of the observed coronal structure and to recognize that individual observables are primarily controlling the value of particular parameters in the model. High confidence in the model as an empirical description of the observed plasma can be realized if the number of measured quantities is sufficient to constrain all of the primary parameters of the modeled plasma. The advantage of the model is that, in simultaneously predicting all of the observable quantities, it takes the relationships among the various physical variables of the plasma into account.

Because the UV, EUV and XUV spectral lines used for coronal diagnostics are optically thin in the corona, an actual observation samples every structure along the line-of-sight. Our study has shown that the contributions from coronal structures lying in the plane of the solar disk ( $\theta = 90^\circ$ ) are enhanced over those of neighboring structures along the line-of-sight. Therefore, it is preferable for the coronal structure of interest to be located in this plane at the time of its observation. Measurements of polar coronal holes are particularly advantageous in this respect. Even in the case of a fairly narrow ( $60^\circ$ ) coronal hole with outflow velocities as large as those in the Munro-Jackson model, the maximum contribution to the observed intensity out to  $\rho = 2.2$  was found to be from the coronal hole (see Figure 5) rather than the surrounding quiet corona. Also, for this example, the observed intensity is highly sensitive to outflow velocity out to beyond  $\rho = 2.5$  and the line profile at  $\rho = 2.0$  is very sensitive to the hydrogen velocity distribution in the hole. Broader coronal holes such as the 1973 polar hole that was discussed by Munro and Jackson (1977), would dominate observations out to higher heights. Narrower coronal hole-like structures of higher density and smaller outflow velocity, such as the one reported by Withbroe *et al.* (1982a), also provide the dominant contribution out to beyond  $\rho = 2.5$ .

Line-of-sight contributions tend to be of more concern for observations of coronal holes than for other coronal structures because they have the smallest densities and the highest outflow velocities. For observations of other coronal structures, the fractional contributions tend to be at least as large as the contributions from the coronal holes considered here and other structures tend to be observable at larger heights. The simulated observations that were considered in this paper have shown that spectroscopic observables are sensitive to the physical parameters of coronal holes and other structures even in representative cases where the structures of interest are surrounded by other regions along the line-of-sight. The examples used here were for relatively small coronal holes and streamers. Larger structures would provide an even larger fraction of the observed intensities.

To demonstrate the feasibility of making EUV spectroscopic observations of the extended corona and to obtain a sample of scientific data, we have observed the intensity and spectral line profile of H I Lyman- $\alpha$  from  $\rho = 1.5$  to 3.5 during three sounding rocket flights. Results for observations of a coronal hole on April 13, 1979 were reported by Kohl *et al.* (1980) and observations of a quiet coronal region from the same rocket flight were discussed by Withbroe *et al.* (1982b). A coronal hole-like structure near the south solar pole was observed on February 16, 1980 and reported by Withbroe *et al.* (1982a). Observation of the polarization and brightness of the white-light corona were made during each flight by a coronagraph of the High Altitude Observatory. During a rocket flight on July 20, 1982, we observed a coronal hole (near the north solar pole) and a nearby streamer. Measurements were made of both the H I Lyman- $\alpha$  profile and the intensities of O VI  $\lambda 1032$  and  $\lambda 1037$ . Although the analysis of those measurements is still in progress, it appears that the data will provide an empirical model of the observed coronal hole that will specify, for the first time, a value for the outflow velocities as well as the random velocities of hydrogen and the electron densities (the latter from white-light data).

Our next EUV spectroscopic measurements of the source region of the solar wind are planned for 1986 on board the Spartan 2 mission which is expected to provide 27 hours for measurements of resonantly scattered H I Lyman- $\alpha$  intensities

and profiles, O VI  $\lambda$ 1032 and  $\lambda$ 1037 intensities, and the intensities and line profiles of the electron scattered component of H I Lyman- $\alpha$ .

This work is supported by NASA Grant NAG5-613 to the Smithsonian Astrophysical Observatory.

#### References

- Allen, C.W., Astrophysical Quantities, 2nd ed. (University of London: Athlone Press, 1963).
- Beckers, J.M., and E. Chipman, The Profile and Polarization of the Coronal Lyman- $\alpha$  Line, Solar Phys., 34, 151, 1974.
- Bommier, V., and S. Sahal-Br  chet, The Hanle Effect of the Coronal L $\alpha$  Line of Hydrogen: Theoretical Investigation, Solar Phys., 78, 157, 1982.
- Gabriel, A.H., Measurements on the Lyman Alpha Corona, Solar Phys., 21, 392, 1971.
- Gabriel, A.H., W.R.S. Garton, L. Goldberg, T.J.L. Jones, C. Jordan, F.J. Morgan, R.W. Nicholls, W.H. Parkinson, H.J.B. Paxton, E.M. Reeves, D.B. Shenton, R.J. Speer, and R. Wilson, Rocket Observations of the Ultraviolet Solar Spectrum During the Total Eclipse of 1970 March 7, Astrophys. J., 169, 595, 1971.
- Hanle, W.,   ber magnetische Beeinflussung der Polarisation der Resonanzfluoreszenz, Z. f. Phys., 30, 93, 1924.
- Hirshberg, J., Composition of the Solar Wind: Present and Past, Rev. Geophys. Space Phys., 13, 1059, 1975.
- Hyder, C.L., The Polarization of Emission Lines in Astronomy II. Prominence Emission-Line Polarization and Prominence Magnetic Fields, Astrophys. J., 141, 1374, 1965.
- Hyder, C.L., and B.W. Lites, H $\alpha$  Doppler Brightening and Lyman- $\alpha$  Doppler Dimming in Moving H $\alpha$  Prominences, Solar Phys., 14, 147, 1970.
- Kohl, J.L., H. Weiser, G.L. Withbroe, R.H. Munro, and G. Noci, New Observations of the Extended Ultraviolet Corona, Bull. Am. Astron. Soc., 14, 976, 1982.
- Kohl, J.L., H. Weiser, G.L. Withbroe, R.W. Noyes, W.H. Parkinson, E.M. Reeves, R.M. MacQueen, and R.H. Munro, Measurements of Coronal Kinetic Temperatures from 1.5 to 3 Solar Radii, Astrophys. J., 241, L117, 1980.
- Kohl, J.L., and G.L. Withbroe, EUV Spectroscopic Plasma Diagnostics for the Solar Wind Acceleration Region, Astrophys. J., 256, 263, 1982.
- Mitchell, A.C.G., and M.W. Zemansky, Resonance Radiation and Excited Atoms, (Cambridge University Press, 1934).
- Munro, R.H., Corona Over a Solar Cycle (Holes, Plumes, Transients, Field Strengths), Proc. of Solar Wind 5, 1983.
- Munro, R.H., and B. Jackson, Physical Properties of a Polar Coronal Hole from 2 to 5  $R_{\odot}$ , Astrophys. J., 213, 874, 1977.
- Noci, G., J.L. Kohl, and G.L. Withbroe, Velocity Sensitivity of Coronal O VI Lines, to be published, 1983.
- Withbroe, G.L., J.L. Kohl, H. Weiser, and R.H. Munro, Probing the Solar Wind Acceleration Region Using Spectroscopic Techniques, Space Sci. Rev., 33, 17, 1982a.
- Withbroe, G.L., J.L. Kohl, H. Weiser, G. Noci, and R.H. Munro, Analysis of Coronal H I Lyman Alpha Measurements from a Rocket on 13 April 1979, Astrophys. J., 254, 361, 1982b.